HHS Public Access

Author manuscript

Acta Biomater. Author manuscript; available in PMC 2020 September 15.

Published in final edited form as:

Acta Biomater. 2019 September 15; 96: 686–693. doi:10.1016/j.actbio.2019.07.028.

Electrically polarized TiO_2 nanotubes on Ti implants to enhance early-stage osseointegration

Amit Bandyopadhyay[*], **Anish Shivaram**, **Indranath Mitra**, **Susmita Bose**

W. M. Keck Biomedical Materials Research Laboratory, School of Mechanical and Materials Engineering, Washington State University, Pullman, Washington, 99164-2920, USA.

Abstract

Ti is characteristically bioinert and is supplemented with modifications in surface topography and chemistry to find use in biomedical applications. The aim of this study is to understand the effects of surface charge on TiO_2 nanotubes (TNT) on Ti implants towards early stage osseointegration. We hypothesize that charge storage on TNT will improve bioactivity and enhance early-stage osseointegration *in vivo*. Commercially pure Ti surface was altered by growing TNT via anodic oxidation followed by the introduction of surface charge through electrothermal polarization to form bioelectret. Our results indicate a stored charge of 37.15±14 mC/cm^2 for TNT surfaces. The polarized TNT (TNT-Ps) samples did not show any charge leakage up to 18 months, and improved wettability with a measured contact angle less than 1°. No cellular toxicity through osteoblast proliferation and differentiation *in vitro* were shown by the TNT-Ps. Enhanced new bone formation at 5 weeks post-implantation for the TNT-Ps in contrast to TNTs was observed *in vivo*. Histomorphometric analyses show ~40% increase in mineralized bone formation around the TNT-P implants than the TNTs at 5 weeks, which is indicative of accelerated bone remodeling cycle. These results show that stored surface charge on TiO_2 nanotubes helped to accelerate bone healing due to early-stage osseointegration *in vivo*.

Graphical Abstract

[*] amitband@wsu.edu.

7.0 Data availability statement

All raw data for this study has been presented in this manuscript.

Conflict of interest

The authors declare no conflict of interest.

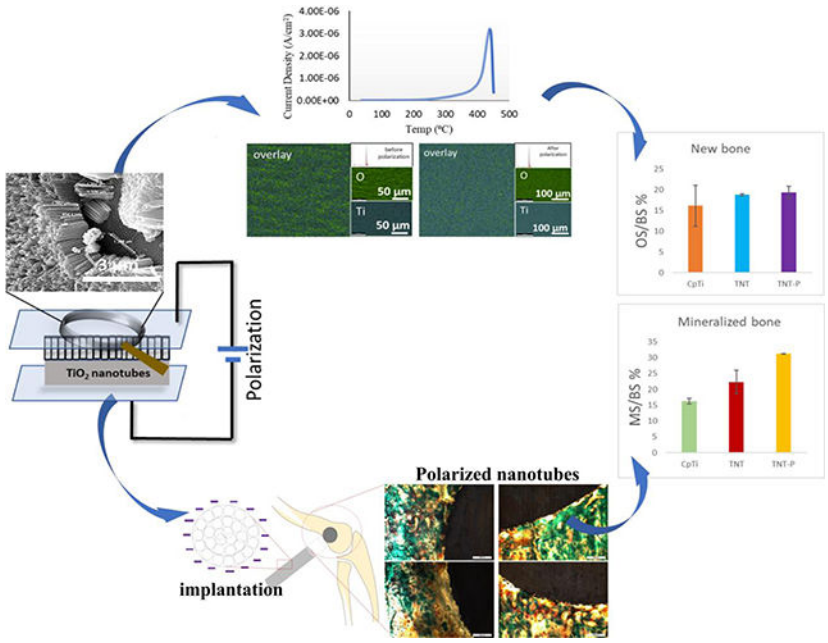

Keywords

Titania nanotubes; polarization; surface charge; surface modification; osseointegration

1.0 Introduction

Biomaterials behave in a complex manner within their immediate physiological surroundings. One way of understanding this behavior is by looking at the material's surface-level interactions with the biological environment. A class of biomaterials called bioelectrets are capacitive in nature which makes them capable of storing electrical charge on their surface. These materials have shown prospect for usage in orthopedic or dental applications because the natural bone is believed to exhibit direct current bio-potential resulting in electrically mediated surface interactions[1]. Clinical results have shown that electrical stimulation can enhance the bone healing process through such interactions between bioelectrets and naturally charged biomolecules [1–3]. This approach towards enhancing cellular response towards a material has been explored in the field of ceramic biomaterials. For example, hydroxyapatite (HAp) bioelectrets have been studied to show the efficiency of charged interactions towards bone regenerative and healing processes *in vitro* as well as *in vivo* [4–11] Preferential *in vitro* osteoblast attachment and proliferation has been demonstrated on polarized HAp compared to non-polarized Hap ceramics [12–18].

Among metallic biomaterials, commercially pure titanium (CpTi) has been widely used in orthopedic and dental biomedical devices. Recent studies have explored the *in vitro* and *in vivo* effect of charge storage on titanium oxide layer formed by micro-arc oxidation of Ti[19]. However, storing electrical charge in architectures like titania nanotubes as a form of surface modification for bio-inert Ti has not been studied. This study intends to investigate the novel integration of bioactive TiO_2 nanotubes (TNT) with charge storage to modify the

surface of CpTi implants towards *in vitro* and *in vivo* biological response. Recently, TNT fabricated by anodic oxidation on CpTi had been explored for its charge storage and electron transport properties in dye-sensitized solar cells [20–22]. TiO_2 layer on the surface of CpTi fundamentally acts as a high-temperature dielectric material and can store charge by the virtue of capacitive effect[23,24]. Since charge storage is essentially a surface phenomenon, TNT aids in increasing the surface area which increases the amount of stored charge as compared to a polished CpTi surface [25,26]. In addition, TNT imparts an increased surface to volume ratio due to its nanoscale topography which lowers the contact angle, making the CpTi surface more hydrophilic [27,28]. This improved surface chemistry and promote osteoblast cell proliferation [29] and upregulation of calcium phosphorous mineralization *in vitro* [30], [31], [32] as well as enhance osseointegration and implant stability *in vivo* [22,33,34].

A convergence of surface chemistry, surface charge, topography, and hydrophilicity are crucial for designing and modification of biomaterial's surface for target specific applications. Thus, in this study, we explored the charge storage effects on TNT towards *in vitro* bone cell-material interactions and *in vivo* early stage osseointegration using a rat distal femur model as shown in Fig. 1. We hypothesize that surface charge storage on TNTs will enhance early-stage osseointegration *in vivo*. To validate our hypothesis, the CpTi surface was anodized to grow TNTs followed by charge storage using electrothermal polarization and evaluated for its biological responses.

2.0 Materials and Methods

2.1 Electrothermal polarization and thermally stimulated depolarization current (TSDC) measurement of TNT

The TNT's were fabricated using CpTi discs (1mm thick and 9.5mm in diameter) using an ethylene glycol-based electrolyte containing 1% (vol) HF at 40V potential difference for 1h. The sample to be anodized was the cathode while a platinum-plate anode was used following protocol established in literature[35]. Samples were rinsed well in D.I. water to wash off any residual HF and then kept at 40°C for 36h for drying. The polarization setup consisted of platinum plates connected with alumel and chromel wires. Polarization was done through the application of a d.c. voltage utilizing a pico-ammeter (Model 6487, Keithley Instruments, OH). The applied voltage was calculated based on the dimensions of the sample discs using equation $E = \frac{V}{d}$, where E= electric field (kV), V= voltage (volts) and d= thickness of the sample disc (cm). The default electric field used for the Keithley instrument is 2kV.

Samples were heated to a polarization temperature (Tp) of 300°C from room temperature at a controlled heating rate of 5°C min^{-1} in a furnace. Once the polarization temperature was reached typically after 1h in 4 step cycles, the TNT samples were applied a d.c. electric field (Ep) of 2 kV cm^{-1} for 1h more. Discs were then cooled to room temperature with the continued application of Ep. Depolarization of the TNT samples was conducted using a similar procedure except during depolarization the temperature of the furnace was raised to 450°C from room temperature while continued application of electric field. Charge storage

was calculated using the area integral equation below as a function of temperature and plotted in a TSDC curve

$$Qp = 1/\beta \int J(T)dT$$

Where, β is the heating rate during TSDC measurement and J(T) is the depolarization current density at temperature T.[4,36]. Field Emission Scanning Electron Microscopy (FESEM) characterization was done before and after polarization of the TNT samples to ensure no thermal degradation from surface morphology analyses of the nanotubes.

2.2 Contact Angle Measurements and X-ray diffraction (XRD) analysis

Contact angle measurements were done through a sessile drop method using a face contact angle set up equipped with a microscope and a camera. A microliter syringe tip was used to put a 0.5–1.0 μl droplet of distilled water on the surface of the sample discs which were pre-adjusted to a certain height to ensure that the droplet made just enough contact with the surface of the disc. The entire process was performed 6 times on each sample and 3 samples from each group were analyzed. An average of the measurements was used to calculate the contact angle. The contact angle measurements were performed on CpTi, TNT and TNT-P samples. Phase analysis was done using X-ray diffraction (XRD) with a Siemens D 500 Kristalloflex diffractometer with Cu-Kα radiation (1.54 Å) at 40 keV and 40 mA, scanning from 2θ values of 30 to 60 degrees at a step size of 0.05 degree and a dwell time of 6s on the surface of the TNT and TNT-P samples.

2.3 Surface chemical analysis

Chemical analysis and elemental mapping of the TNT surface before and after polarization was performed using Energy Dispersive Analysis of X-Rays (EDAX) [EDAX element EDS system, AMETEK Inc. Berwyn, PA] in conjunction with Tescan Vega3 SEM (Tescan USA, Inc. Warrendale PA). The TNT and TNT-P surfaces were analyzed through Smart Element Mapping and Spectrum, Utilities software for chemical composition under 30kV and fixed working distance of 13.6mm.

2.4 *In vitro* and *in vivo* study

2.4.1 Cellular attachment and cytocompatibility evaluation—

Circular discs samples of 12.5mm in diameter and 3mm in thickness were used to study bone-cell materials interaction (5 samples from group TNT and TNT-P) with human fetal osteoblast (hFOB) (American Type Culture Collection (ATCC), Manassas, VA) cells for 3, 7- and 11-days post-sterilization by autoclaving at 121°C for 60 min. Cells were seeded onto the disc samples (initial seeding intensity: 15000/well) in 24 well-plates and Ham's F12 Medium and Dulbecco's Modified Eagle's Medium (DMEM/F12, Sigma, St. Louis, MO) mixture along with 2.5 mM L-glutamine was used as the nutrient growth medium. The growth medium was augmented with 10% fetal bovine serum (ATCC, Manassas, VA) added with 0.3 mg/ml G418 sulfate salt (Sigma Aldrich) and the cell plates were maintained at 34°C under a 5% CO_2 environment in an incubator as recommended by the ATCC protocol for this cell line. Fresh media was added every 2 days throughout the experiment.

MTT (3-(4, 5-dimethylthiazol-2-yl)-2, 5-diphenyl tetrazolium bromide) assay was performed to evaluate cell proliferation. The MTT (Sigma Aldrich) salt was dissolved in phosphate buffer saline to prepare a 5mg/ml solution which was then sterilized using a filter sterilization unit through 0.2 μm pore filter paper. 3 samples from each group and triplicate measurements from each sample were assessed for MTT assay. Differentiation behavior of osteoblasts was evaluated from alkaline phosphatase (ALP) activity using a SensoLyte® pNPP Alkaline Phosphatase assay (AnaSpec, Fremont, CA, USA) at 7 and 11 days. The cells were lysed by Triton X-100 (Anaspec, Inc., Fremont, CA, USA) into the kit and reacted with working solution followed by measurement of absorbance at 405nm. A fixative consisting of 2% paraformaldehyde/ 2% glutaraldehyde in 0.1 M phosphate buffer was used to fix the samples for SEM overnight at 4°C. Post fixation, the samples were rinsed in triplicates with a PBS buffer to eliminate any remaining fixative followed by addition of 2% osmium tetroxide (OsO_4) and were left for 2h at room temperature. After rinsing out the OsO_4 in triplicate using ddH_2O, serial dehydration of the fixed samples was performed using ethanol (30%, 50%, 70%, 95% and thrice with 100%) followed by critical drying using hexamethyldisilane (HMDS) to eliminate artifacts such as shrinkage and collapse of surface structures under surface which is common in air drying after ethanolic dehydration. The samples were gold coated prior to FESEM imaging of the surface morphology of the cells.

2.4.2 Surgery and implantation procedure—Male Sprague-Dawley rats with average weights between 300 and 320g were used for the *in vivo* study. Surgeries were performed on a distal femur defect model. Rats were housed in individual cages for at least 6 days in a temperature and humidity-controlled room for acclimation prior to surgery. Animals were anesthetized using a prescribed dose of IsoFlo® with oxygen and time to time monitored by pedal reflex and respiration rate to maintain proper surgical anesthesia. Bilateral defects in the distal femurs were created using a drill bit similar to that of the implant (length x diameter: 5mm x 3mm) followed by a saline rinse to eliminate any remaining bone fragments. 2 implants (each in one femur) were implanted in a single rat. Implant rods for each composition were statistically distributed in the rats following a complete randomized block design. Post-procedure, the fascia over the incision was sutured using undyed braided coated MONOCRYL-polyglactin 910 (Ethicon Inc., Somerville, NJ, USA) and the outer skin was stapled using surgical staples. Antiseptic (betadine solution) was applied over the closed incision to prevent post-surgical primary infection. Buprenorphine (0.03 mg kg^{-1}) were administered to the rats 45 minutes prior to surgery as a pain reducing medication. An anti-inflammatory analgesic in the form of subcutaneous meloxicam (0.2 mg kg^{-1}) was administered after surgery. At the end of 5 weeks, rats were euthanized by carbon dioxide overdose followed by cervical dislocation as a secondary measure. Institutional Animal Care and Use Committee (IACUC) of Washington State University (Pullman, WA) approved protocol was followed to perform the experimental and surgical procedure.

2.4.3 μCT analysis and interfacial strength measurements—μCT images were acquired from X-ray energy source on the IVIS® Spectrum CT. Samples were placed in the sample holder parallel to the axis of the sample holder. Living Image® Software 4.4 was used to generate three-dimensional images from the layerwise sample scans using 40μm

voxel size and 150μm pixel size resolution. Two samples (cylindrical rods; dia- 3mm, height- 5mm) for each composition was scanned using μCT measurements. The harvested explants were wrapped in sterile saline gauze before taking to the push out experiment facility. Push out tests were performed to evaluate shear modulus at the bone-implant interface using a 136.07kg load cell (Instron 3433) at a cross-head speed of 0.33 mm/sec. Shear modulus can be used to understand bond strength characteristics between the implant surface and the surrounding host tissue. The highest slope from shear stress vs shear strain plot was used to calculate shear modulus. Proper clamping arrangements were used to keep the sample in place during the course of the experiment vis-à-vis prevent any translation in X, Y direction while the load cell moved along the Z axis.

2.4.4 Histology and SEM characterization—For histological analysis, after fixation in 10% formalin for 72h and series dehydration of ethanol and acetone, bone-implant samples were embedded in Spurrs resin. They were further sliced into thin sections (3 sections from each sample and 2 samples from each composition) using a diamond saw. After mounting on glass slides, modified Masson Goldner's trichrome staining was used for the histology analysis. Stained cross sections of the resin-embedded implant-tissue were observed under an optical microscope (Olympus BH-2, Olympus America Inc., USA) and SEM (FEI Quanta 200, FEI Inc., OR, USA), at a low voltage of 5V. Attained optical images were used for histomorphometric analysis, which was carried out using Gimp 2.8 software. Standardized region of interest (ROI) [37] of 0.25 mm thickness was projected radially from the bone/implant interface for the calculations, as shown in Fig. 2. Osteoid colors – red/orange and mineralized bone colors – greenish-blue (individually manipulated) were isolated from other spectrum colors and osteoid surface per bone surface (OS/BS) and mineralized surface per bone surface(MS/BS) percent were calculated [38] (see supplementary Fig. 1).

2.5 Statistical analysis

Histomorphometric analysis, MTT assay and ALP assay demonstrated in this study have been reported as the mean ± standard deviation. Statistical analysis was performed using a two-way ANOVA model followed by multiple comparison correction using TUKEY-KRAMER model and $\alpha = 0.05$. A P-value $< \alpha$ was marked as significant.

3.0 Results

3.1 Electrothermal polarization and thermally stimulated depolarization current (TSDC) measurement of TNT

TNT was grown using ethylene glycol-based electrolyte resulted in nanotubes of ~1μm in length and ~105nm in diameter, as shown in Fig. 3a. Electrothermal polarization for all samples was carried at 300°C by passing a constant electric field of 2kV cm^{-1} and depolarized at 450°C. Fig. 3b represents the TSDC spectra of TNT-P. The maximum stored charge in the TNT samples was calculated to be 37.15±14 mC/cm^2 at a temperature of 390.69±30°C (n=4). Fig. 3d. gives a comparison between the specific capacitance for electrothermally polarized TNT with the maximum stored charge with the literature values for specific capacitance calculated for TNTs used as a supercapacitor[39,40]. TNT samples were characterized before and after electrothermal polarization to ensure the heat treatment

does not damage or thermally degrade the nanotubes. Fig. 3a and 3c show the SEM images of TNT before and after electrothermal polarization, respectively, indicating no signs of thermal degradation.

3.2 XRD analysis and contact angle measurements

XRD analysis for the TNT and TNT-P sample surfaces matched with Ti (JCPDS #44–1294). No other phases were detected (Fig. 3e) suggesting as-grown TNTs were all amorphous in nature. Contact angle measurements were performed using DI water to study surface wettability properties due to electrothermal polarization. Fig. 4a shows contact angle values for all samples. The contact angle for TNT-P samples was found to be 0°, showing excellent surface wettability compared to all other samples. Such results confirm that electrothermal polarization improves the hydrophilicity of TNT samples, which should also enhance biocompatibility for these surfaces by rendering them more favorable for cellular attachment in a physiological fluid environment.

3.3 Surface chemical analysis

EDAX analysis of surface chemistry of TNT before and after polarization (TNT-P) showed the presence of only Ti and oxygen (O) and no signatures of hydrocarbon and fluoride contamination (area analysis spectrum). Fig 3f. shows uniform distribution of Ti and O throughout the entire examined surface evident from the elemental maps. Atomic % of Ti and O were observed to be 42.89±1 and 46.45±11 respectively for TNT and 41.35±1 and 58.47±11 respectively for TNT-P.

3.4 *In vitro* study

MTT, ALP Assay, and FESEM analysis—MTT, ALP assays and SEM morphological analysis of osteoblast proliferation, differentiation and attachment were performed for TNT and TNT-P samples. The rationale for conducting an MTT (Fig. 4b) and ALP (Fig. 4c) assays was to evaluate cellular toxicity of the compositions. The SEM micrographs (Fig 4d) show well-attached osteoblasts on both samples through the presence of filopodial extensions. Substrate surface coverage with higher cell density was noticed in TNT-P compared to TNT from day 3 to day 11. MTT assay shows osteoblast viability as a function of optical density for the compositions. TNT-P shows significantly higher cell viability than TNT at day 7 and 11. ALP activity exhibits higher osteoblast differentiation at day 7 for TNT-P, although, ALP activity plateaus at day 11 for both compositions.

3.5 *In vivo* study

Proper lodging of the implants was observed from the harvested samples after 5 weeks of implantation through CT scan analysis (Fig. 5a). The shear modulus from push out experiments for TNT-P (123.26 ± 2 MPa) is shown to be significantly higher than that of the TNT (83.28 MPa) or the CpTi (39.21 ± 7 MPa). These values indicate excellent early stage interfacial bonding between the implant and the host tissue. Furthermore, the observation for TNT-P was reaffirmed by bone fracture during the push-out test, which also indicates better bonding between the implant and the surrounding tissue. To obtain a better understanding of the bonding at the implant-bone interface, SEM characterization was performed for the

stained samples. Fig. 5b shows the SEM images of all samples focusing on interfacial bonding. It could be observed that the control CpTi samples show poor bonding due to the presence of significant gaps. The TNT-P samples show better interlocking of cellular surface with implant surface at the bone-implant interface indicative of early-stage osseointegration. Biocompatibility of the TNT-P implants and the effect of surface charge on new bone formation were studied through histological evaluation of the implant-bone interface. Fig. 5c shows the histology micrographs of bone-tissue interface for CpTi, TNT and TNT-P. The osteoid formation is represented by the orange-red region, while the greenish-blue region indicates mineralized bone, and the bluish-black spots represent nuclei from Masson Goldner's Trichrome staining procedure. Qualitative analyses of osteoid formation from the histology micrographs show no concerns related to cytotoxicity from TNT-P.

Histomorphometric evaluation (Fig. 5d) was performed using Gimp 2.8 software for osteoid surface (OS) and mineralized bone surface (MS) as percentages of total bone surface (BS) i.e., OS/BS% and MS/BS% around the implants. The calculations were done in triplicates for each histology image (see supplementary Fig. 1). The evaluation of OS/BS % shows comparable osteoid formation for the TNT and TNT-Ps but a higher percentage of osteoid formation in contrast to CpTi. On the other hand, the MS/BS % show a higher amount of mineralized bone formation for the TNT-Ps as compared to the TNT and CpTi.

4.0 Discussion

The surface of a biomedical device comes first in contact with the physiological surroundings right after implantation. Therefore, looking at surface interactions between material and host tissue becomes a decisive factor in determining the performance of the implant. From a long-term perspective, efficiency, interfacial stability, and longevity of biomedical devices largely depend on their surface property and subsequent modifications. In this study, a novel integration of surface modification techniques such as TNT and storage of surface charge has been evaluated towards enhancing biological response of CpTi implants. The results suggest that osteoid formation strongly responds to TNT-P surfaces, thereby enhancing early stage osseointegration at the bone-implant interface *in vivo*.

Taking into account the enhanced biological response of charged ceramic surfaces [5], this study explored the *in vitro* and *in vivo* interactions between electrothermally polarized TNT and host bone tissue. In the light of this, our TNT samples before and after polarization were evaluated for identification of any phase change due to thermal treatment during polarization. XRD analysis (Fig. 3e) revealed Ti peaks for both the samples without the detection of any other observable phases. This indicates that heat treatment during polarization does not affect the amorphous TNT. No evidence of any crystallization of TNT is seen, which typically happens above 450°C[35]. In addition to this we have also explored the possibility of any contamination using EDS area analysis for chemical composition of TNT and TNT-P. Spectrum (Fig 3f) shows the presence of Ti and O peaks with no additional peaks related to any hydrocarbon and fluoride contamination. Surface chemical analysis of TNT and TNT-P showed uniform distribution of Ti and O on the examined surfaces corroborating the formation of TiO_2 layer. Recent study on ALD (atomic layer deposition) grown TiO2 layer elucidates the mechanism of reactive oxygen species formation and

decrease in defect density in heat treated TiO2 surfaces which in turn improves stability of such oxide films[41]. It is noteworthy that the TNT grown surfaces as reported from EDS are not stoichiometric ($TiO_{2-\delta}$) with ~ 42% (atomic) Ti as opposed to 33% in a stoichiometric TiO_2 which can be accounted for interstitial Ti or O vacancies (~46% in TNT). The oxygen enrichment for the TNT-P (~ 58%) surface after thermal exposure during polarization can be attributed to the formation of Ti suboxides (Ti^{3+} and Ti^{2+}) as well as space-charge effect resulting in migration of excess electrons towards the surface of TNT-P. This in turn results in the formation of reactive oxygen species (O^-) at the electrode-TNT interface and reduction in defect density as follows,

$$1/2O^2 + 2e^- \rightarrow O^{2-} \text{and } TiO_{2-\delta} + O^{2-} \rightarrow TiO_{2-\alpha} (\alpha < \delta)$$

TSDC results for TNT-P showed charge storage of 37.15±14 mC/cm^2 which was ~40 times higher than the values reported in the literature for ceramic surfaces as well as anatase TiO_2 layers (Fig. 3b). For example, HAp implants have been reported for stored charge values ranging between 0.08μCcm^{-2} to 1.2 mCcm^{-2} through electrothermal polarization[12–14,42]. The effects on polarizability of HAp bioelectrets have also been explored under varying poling temperatures from 250°C to 500°C, which showed significant variations in stored charge value from 0.5 to 45 μCcm^{-2} [15]. Recently, *in vivo* effect of polarized anatase TiO_2 formed using micro-arc oxidation has also been reported with a maximum stored charge in polarized treatments to be 28.4 μC/cm^2.

Considering higher value of stored charge in TNT, specific capacitance was calculated to 0.97 mF/cm^2, which is close to the values reported in the literature for supercapacitor-based applications [20], [39](Fig. 3d). In a quest for understanding the enhancement of stored charge in TNT compared to ceramic surfaces, we explored the proposed mechanisms. Heat treatment of TNT reduces the band gap energy to 2.4eV due to higher conversion of Ti^{4+} to Ti^{3+} [6], [7,24]. This facilitates the ease of space-charge polarization which leads to the formation of a Helmholtz double-layer like charge concentration distribution at the electrode-TNT interface[43]. The high specific surface of TNT aids in higher contact area as well as ordered array of nanotubes reduce the disturbance from interparticle connections providing direct contact for electron transfer[24]. This charge concentration distribution occurs with the formation of electron-hole pairs[25]. Highly ordered structure of TNT and subsequent heat treatment play a role in suppressing the surface recombination of electron and holes due to fewer defects. Studies have shown that TNT aid in delaying recombination time constants by trapping the generated electron at the center of the tubular structure, thereby providing TNT with pseudo-capacitor characteristics[25,26].

The TNT-P samples were observed for charge storage through periodic TSDC measurements. We found no significant charge leakage even after 18 months post-polarization. Keeping in mind, the depolarization temperature is 450°C (Fig. 3b), that indicates these implants can efficiently perform in a physiological system (~ 37°C) without any likelihood of depolarization resulting in energy discharge.

The focus of this study was to understand the influence of surface charge in TNT towards *in vitro* osteogenic as well as *in vivo* early stage osseointegrative properties. It is important to recognize that, since XRD analysis did not reveal the presence of any detectable phases other than Ti, biological response of the samples was evaluated as a function of surface charge only. We observed *in vitro* osteoblast attachment, proliferation, and differentiation through SEM, MTT and ALP assays in order to evaluate any cellular toxicity for TNT and TNT-P samples because of their harsh synthesis environment such as presence of HF in the electrolyte. Extensive biocompatibility studies have already been conducted for CpTi which show no cytotoxicity in untreated conditions. SEM micrographs (Fig. 4d) show the formation of cellular micro-extensions called filopodia and adherence of the cells to each other as well as a substrate in both TNT and TNT-P samples. More flattened architecture of osteoblasts was observed on TNT-P samples in contrast to lesser cell spreading on TNT after 7 and 11 days of culture. Under proliferated cylindrical cells coupled with under-developed filopodial extensions were seen on the TNT (day 3) surface than TNT-P samples. These results are in accordance with the contact angle measurements (Fig. 4a), where TNT-P samples revealed complete wetting. ALP assay (Fig. 4c) suggests TNT-P aiding in initial osteoblast differentiation at day 7 which eventually plateaus at day 11 for TNT and TNT-P. However, MTT results (Fig. 4b) show higher osteoblast proliferation at day 7 and day 11 for TNT-P than TNT. This indicates that TNT-P exhibits early osteogenesis and proliferation (from day 3 to day 7) while at a later stage TNT-P helps in osteoblast differentiation (from day 7 to day 11). The high values of viable densities with better cell morphology and adherence on TNT-P surfaces suggest no cellular toxicity due to surface charge or synthesis conditions as a function of no inhibition in osteoblast growth.

In vivo osseointegration and new bone formation study was performed in a rat distal femur model for 5 weeks since our focus was only to understand the early stage osseointegration. Our results showed early stage osseointegrative properties of TNT-P surfaces compared to TNT and CpTi surfaces. High interfacial integration strength for TNT-P surfaces could be seen from the shear modulus value of 123.26 ± 17 MPa, which resulted in bone fracture during push out experiments due to excellent bone-tissue integration. Fig. 5c shows optical micrographs of tissue sections of bone-implant interface for CpTi, TNT and TNT-P stained with modified Masson-Goldner's Trichrome. There is no scar tissue formation around the implant at the interface which is often a result of undesirable immune response[44], in the form of aseptic loosening. Almost seamless interfacial interlocking of bone and implant for TNT-P evident from SEM images (Fig. 5b) as well as close apposition of bone and implant from micro-CT (Fig. 5a) validates excellent biocompatibility of TNT-P implants. Qualitative histological assessment of the compositions revealed comparable OS/BS% for TNT and TNT-Ps, which were higher than CpTi. Moreover, Fig. 5d shows the histomorphometrical evaluation of OS/BS% and MS/BS%. Histomorphometry results suggest a significantly higher mineralized bone formation for the TNT-Ps as compared to TNT (39.94% increase) and CpTi (92% increase) proving the efficacy of the TNT-P to not only aid in osteoid formation but also accelerate bone remodeling cycle through active maturation of osteoid into mineralized bone tissue. Better tissue interlocking at the host bone-implant interface for the TNT-P samples can be attributed to a combined effect of nanotube structure and morphology along with additional surface charge. This can be better elaborated by

considering their individual contributions. Studies have explored the effect of negatively poled and positively poled ceramic surfaces on in vitro cell-material interaction where they have reported negatively charged surfaces to be more favorable for cellular (osteoblast) attachment and proliferation due to preferential charge interactions with charged biomolecules in bone and physiological environment. On the other hand, the presence of nanotubes enhances the wettability of the surface of the implant due to the higher surface area to the volume ratio, leading to the recruitment of histone, albumin and inorganic calcium ions[36].

In summary, our findings of accelerated early stage bone healing through the formation of active mineralization front in TNT-P samples corroborates with expected observation from a charged material-cell interaction. Compared to TNT, TNT-P showed better *in vitro* and *in vivo* performance due to enhanced interfacial interactions with biological surroundings. Our results suggest TNT-P can help in enhancing the early stage osseointegrative properties of CpTi implants through a correlation of surface topography, surface charge, hydrophilicity and surface chemistry. Our results necessarily infer that growing titania nanotubes can be extended to any Ti alloys like an α-β alloy such as Ti6Al4V. However, that would involve a different electrolyte chemistry as well as time and electrode voltage. Although nanotube architecture would vary from an α alloy to a β alloy and α, β alloy, the polarization aspect does not change meaning, if a surface is favorable to grow nanotubes, subsequent polarization can be implemented to store charge on such surfaces. These findings can pave directions for integrated biomedical orthopedic or dental devices which bridges gaps between surface modified and patient-specific 3D printed implants towards providing a comprehensive faster healing [45].

5.0 Conclusions

TiO_2 nanotubes (TNTs) were grown electrochemically on Ti surface of approximately 1 μm long and 100 nm diameter using ethylene glycol medium containing HF. Surface charge of ~ 40 mC/cm^2 was stored on polarized TNT using electrothermal polarization method. Contact angle measurements showed improved hydrophilicity for TNT-P over TNT. Enhanced osteoblast attachment, proliferation, and differentiation *in vitro* revealed the biocompatibility and efficiency of TNT-P towards improved cell-materials interaction. Push out tests, SEM micrographs and histological characterizations showed enhanced interfacial shear modulus values for TNT-P, revealing accelerated healing with improved interfacial bonding between the implant and osseous tissue. Electrothermally polarized TNT is a potential candidate for surface modified metallic implants in bone tissue engineering applications for improved early stage osseointegration and faster healing particularly for patients with compromised bone.

Supplementary Material

Refer to Web version on PubMed Central for supplementary material.

Acknowledgements

Research reported in this publication was supported by the National Institute of Arthritis and Musculoskeletal and Skin Diseases of the National Institutes of Health under Award Number R01 AR067306–01A1. The content is solely the responsibility of the authors and does not necessarily represent the official views of the National Institutes of Health.

8.0 References

[1]. Friedenberg ZB, Brighton CT, Bioelectric potentials in bone, JBJS. 48 (1966) 915–923.

[2]. Bassett CAL, Pawluk RJ, BECKER RO, Effects of electric currents on bone in vivo, Nature. 204 (1964) 652. [PubMed: 14236279]

[3]. Mascarenhas S, The electret effect in bone and biopolymers and the bound-water problem, Ann. N. Y. Acad. Sci. 238 (1974) 36–52.

[4]. Nakamura S, Takeda H, Yamashita K, ceramics J Appl. Phys. 89 (2001) 5386–5392.

[5]. Ueshima M, Nakamura S, Yamashita K, Huge, millicoulomb charge storage in ceramic hydroxyapatite by bimodal electric polarization, Adv. Mater. 14 (2002) 591–595.

[6]. Kumar D, Gittings JP, Turner IG, Bowen CR, Bastida-Hidalgo A, Cartmell SH, Polarization of hydroxyapatite: Influence on osteoblast cell proliferation, Acta Biomater. 6 (2010) 1549–1554. [PubMed: 19914408]

[7]. Tarafder S, Bodhak S, Bandyopadhyay A, Bose S, Effect of electrical polarization and composition of biphasic calcium phosphates on early stage osteoblast interactions, J. Biomed. Mater. Res. B Appl. Biomater. 97 (2011) 306–314. [PubMed: 21442744]

[8]. Bodhak S, Bose S, Bandyopadhyay A, Role of surface charge and wettability on early stage mineralization and bone cell–materials interactions of polarized hydroxyapatite, Acta Biomater. 5 (2009) 2178–2188. [PubMed: 19303377]

[9]. Tofail SA, Bauer J, Electrically polarized biomaterials, Adv. Mater. 28 (2016) 5470–5484. [PubMed: 27122372]

[10]. Tofail SAM, Gandhi AA, Electrical Modifications of Biomaterials' Surfaces: Beyond Hydrophobicity and Hydrophilicity, Biol. Interact. Surf. Charge Biomater. (2011) 3–14.

[11]. Hempel U, Wolf-Brandstetter C, Scharnweber D, Interactions of Bone-forming Cells with Electrostatic Charge at Biomaterials' Surfaces, in: Biol. Interact. Surf. Charge Biomater., Royal Society of Chemistry, 2011: pp. 107–121.

[12]. Becker RO, Bioelectric factors controlling bone structure, Bone Biodyn (1964).

[13]. Lavine LS, Lustrin I, Shamos MH, Moss ML, The influence of electric current on bone regeneration in vivo, Acta Orthop. Scand. 42 (1971) 305–314. [PubMed: 5144193]

[14]. Kim IS, Song JK, Zhang YL, Lee TH, Cho TH, Song YM, Kim DK, Kim SJ, Hwang SJ, Biphasic electric current stimulates proliferation and induces VEGF production in osteoblasts, Biochim. Biophys. Acta BBA-Mol. Cell Res. 1763 (2006) 907–916.

[15]. Meng S, Zhang Z, Rouabhia M, Accelerated osteoblast mineralization on a conductive substrate by multiple electrical stimulation, J. Bone Miner. Metab. 29 (2011) 535–544. [PubMed: 21327884]

[16]. Ercan B, Webster TJ, The effect of biphasic electrical stimulation on osteoblast function at anodized nanotubular titanium surfaces, Biomaterials. 31 (2010) 3684–3693. [PubMed: 20149926]

[17]. Yamashita K, Kitagaki K, Umegaki T, Thermal instability and proton conductivity of ceramic hydroxyapatite at high temperatures, J. Am. Ceram. Soc. 78 (1995) 1191–1197.

[18]. Nakamura M, Nagai A, Hentunen T, Salonen J, Sekijima Y, Okura T, Hashimoto K, Toda Y, Monma H, Yamashita K, Surface electric fields increase osteoblast adhesion through improved wettability on hydroxyapatite electret, ACS Appl. Mater. Interfaces. 1 (2009) 2181–2189. [PubMed: 20355852]

[19]. Nozaki K, Wang W, Horiuchi N, Nakamura M, Takakuda K, Yamashita K, Nagai A, Enhanced osteoconductivity of titanium implant by polarization-induced surface charges, J. Biomed. Mater. Res. A. 102 (2014) 3077–3086. doi:10.1002/jbm.a.34980. [PubMed: 24123807]

[20]. Cargnello M, Montini T, Smolin SY, Priebe JB, Jaén JJD, Doan-Nguyen VV, McKay IS, Schwalbe JA, Pohl M-M, Gordon TR, Engineering titania nanostructure to tune and improve its photocatalytic activity, Proc. Natl. Acad. Sci. 113 (2016) 3966–3971. [PubMed: 27035977]

[21]. Devlin RC, Khorasaninejad M, Chen WT, Oh J, Capasso F, Broadband high-efficiency dielectric metasurfaces for the visible spectrum, Proc. Natl. Acad. Sci. 113 (2016) 10473–10478. [PubMed: 27601634]

[22]. Kulkarni M, Mazare A, Park J, Gongadze E, Killian MS, Kralj S, von der Mark K, Iglič A, Schmuki P, Protein interactions with layers of TiO2 nanotube and nanopore arrays: Morphology and surface charge influence, Acta Biomater. 45 (2016) 357–366. [PubMed: 27581395]

[23]. Salari M, Aboutalebi SH, Chidembo AT, Nevirkovets IP, Konstantinov K, Liu HK, Enhancement of the electrochemical capacitance of TiO 2 nanotube arrays through controlled phase transformation of anatase to rutile, Phys. Chem. Chem. Phys. 14 (2012) 4770–4779. [PubMed: 22382869]

[24]. Salari M, Konstantinov K, Liu HK, Enhancement of the capacitance in TiO 2 nanotubes through controlled introduction of oxygen vacancies, J. Mater. Chem. 21 (2011) 5128–5133.

[25]. Zhu K, Neale NR, Miedaner A, Frank AJ, Enhanced charge-collection efficiencies and light scattering in dye-sensitized solar cells using oriented TiO2 nanotubes arrays, Nano Lett. 7 (2007) 69–74. [PubMed: 17212442]

[26]. Fabregat-Santiago F, Barea EM, Bisquert J, Mor GK, Shankar K, Grimes CA, High carrier density and capacitance in TiO2 nanotube arrays induced by electrochemical doping, J. Am. Chem. Soc. 130 (2008) 11312–11316. [PubMed: 18671396]

[27]. Brammer KS, Oh S, Cobb CJ, Bjursten LM, van der Heyde H, Jin S, Improved bone-forming functionality on diameter-controlled TiO2 nanotube surface, Acta Biomater. 5 (2009) 3215–3223. [PubMed: 19447210]

[28]. Das K, Bandyopadhyay A, Bose S, Biocompatibility and in situ growth of TiO2 nanotubes on Ti using different electrolyte chemistry, J. Am. Ceram. Soc. 91 (2008) 2808–2814.

[29]. Bjursten LM, Rasmusson L, Oh S, Smith GC, Brammer KS, Jin S, Titanium dioxide nanotubes enhance bone bonding in vivo, J. Biomed. Mater. Res. A. 92 (2010) 1218–1224. [PubMed: 19343780]

[30]. Bobyn JD, Pilliar RM, Cameron HU, Weatherly GC, The optimum pore size for the fixation of porous-surfaced metal implants by the ingrowth of bone., Clin. Orthop. (1980) 263–270.

[31]. Webster TJ, Ejiofor JU, Increased osteoblast adhesion on nanophase metals: Ti, Ti6Al4V, and CoCrMo, Biomaterials. 25 (2004) 4731–4739. [PubMed: 15120519]

[32]. Ward BC, Webster TJ, Increased functions of osteoblasts on nanophase metals, Mater. Sci. Eng. C. 27 (2007) 575–578.

[33]. Das K, Bose S, Bandyopadhyay A, TiO2 nanotubes on Ti: Influence of nanoscale morphology on bone cell–materials interaction, J. Biomed. Mater. Res. A. 90 (2009) 225–237. [PubMed: 18496867]

[34]. Bandyopadhyay A, Shivaram A, Tarafder S, Sahasrabudhe H, Banerjee D, Bose S, In vivo response of laser processed porous titanium implants for load-bearing implants, Ann. Biomed. Eng. 45 (2017) 249–260. [PubMed: 27307009]

[35]. Shivaram A, Bose S, Bandyopadhyay A, Thermal degradation of TiO2 nanotubes on titanium, Appl. Surf. Sci. 317 (2014) 573–580.

[36]. Bodhak S, Bose S, Bandyopadhyay A, Electrically polarized HAp-coated Ti: In vitro bone cell–material interactions, Acta Biomater. 6 (2010) 641–651. [PubMed: 19671456]

[37]. Vandeweghe S, Coelho PG, Vanhove C, Wennerberg A, Jimbo R, Utilizing micro-computed tomography to evaluate bone structure surrounding dental implants: A comparison with histomorphometry, J. Biomed. Mater. Res. B Appl. Biomater. 101 (2013) 1259–1266. [PubMed: 23661363]

[38]. He T, Cao C, Xu Z, Li G, Cao H, Liu X, Zhang C, Dong Y, A comparison of microCT and histomorphometry for evaluation of osseointegration of PEO-coated titanium implants in a rat model, Sci. Rep. 7 (2017) 16270. [PubMed: 29176604]

[39]. Wu H, Li D, Zhu X, Yang C, Liu D, Chen X, Song Y, Lu L, High-performance and renewable supercapacitors based on TiO2 nanotube array electrodes treated by an electrochemical doping approach, Electrochimica Acta. 116 (2014) 129–136.

[40]. Wu H, Xu C, Xu J, Lu L, Fan Z, Chen X, Song Y, Li D, Enhanced supercapacitance in anodic TiO2 nanotube films by hydrogen plasma treatment, Nanotechnology. 24 (2013) 455401. [PubMed: 24141177]

[41]. Hannula M, Ali-Löytty H, Lahtonen K, Sarlin E, Saari J, Valden M, Improved Stability of Atomic Layer Deposited Amorphous TiO2 Photoelectrode Coatings by Thermally Induced Oxygen Defects, Chem. Mater. 30 (2018) 1199–1208. doi:10.1021/acs.chemmater.7b02938. [PubMed: 30270988]

[42]. Wu J, Dittrick S, Rudenko P, Bose S, Bandyopadhyay A, Characterization of calcium phosphate reinforced Ti-6Al-4V composites for load-bearing implants, Biomater. Sci. Process. Prop. Appl. III Ceram. Trans. Vol. 242 (2013) 1–9.

[43]. Fu C, Savino K, Gabrys P, Zeng A, Guan B, Olvera D, Wang C, Song B, Awad H, Gao Y, Hydroxyapatite thin films with giant electrical polarization, Chem. Mater. 27 (2015) 1164–1171.

[44]. Tang L, Eaton JW, Inflammatory responses to biomaterials, Am. J. Clin. Pathol. 103 (1995) 466–471. [PubMed: 7726145]

[45]. Bose S, Ke D, Sahasrabudhe H, Bandyopadhyay A, Additive manufacturing of biomaterials, Prog. Mater. Sci. (2017).

To improve surface bioactivity of metallic biomaterials, various approaches have been proposed and implemented. Among them, stored surface charge has been explored to enhance biological responses for hydroxyapatite ceramics where charged surfaces show favorable bone tissue ingrowth. However, surface charge effects have not yet been explored as a way to mitigate bio-inertness of titanium. This study intends to understand novel integration of bioactive titania-nanotubes and charge storage as surface modification for titanium implants. Our results show excellent biological response due to surface charge on titania-nanotubes offering possibilities of faster healing particularly for patients with compromised bone health.

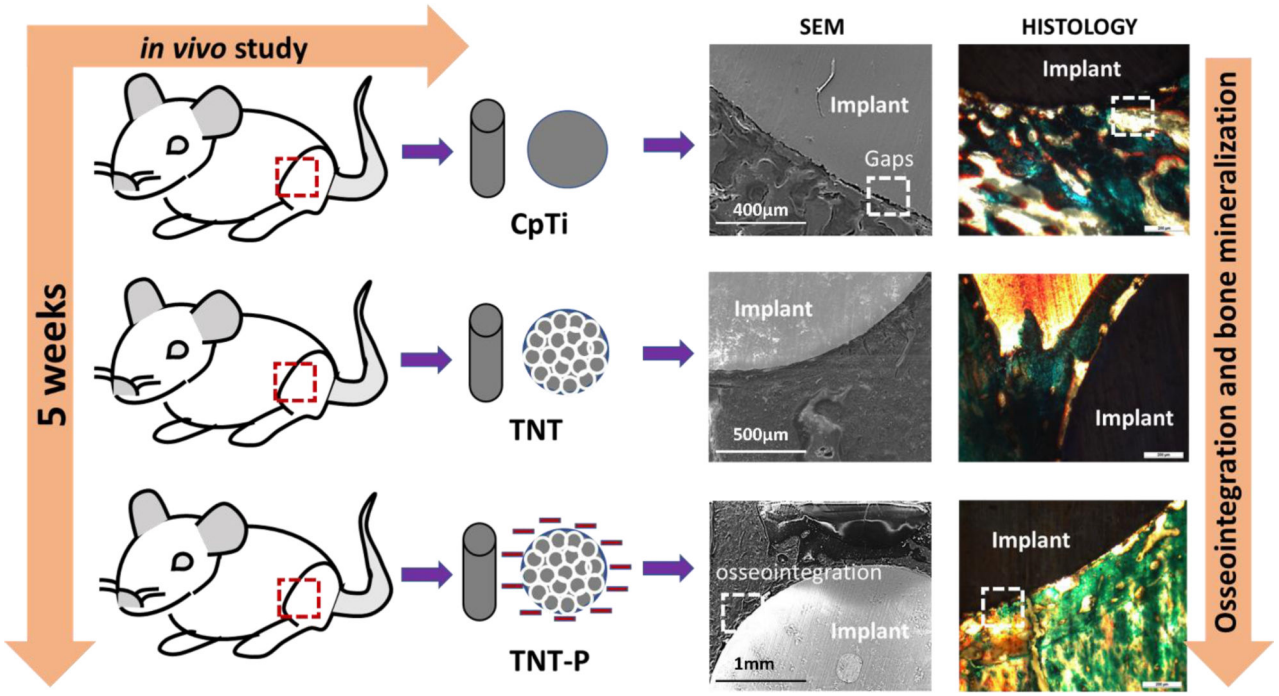

Fig. 1:

Schematic illustration of osseointegration in TNT-P compared to CpTi and TNT, evaluated through a 5-week in vivo study in rat distal femur model.

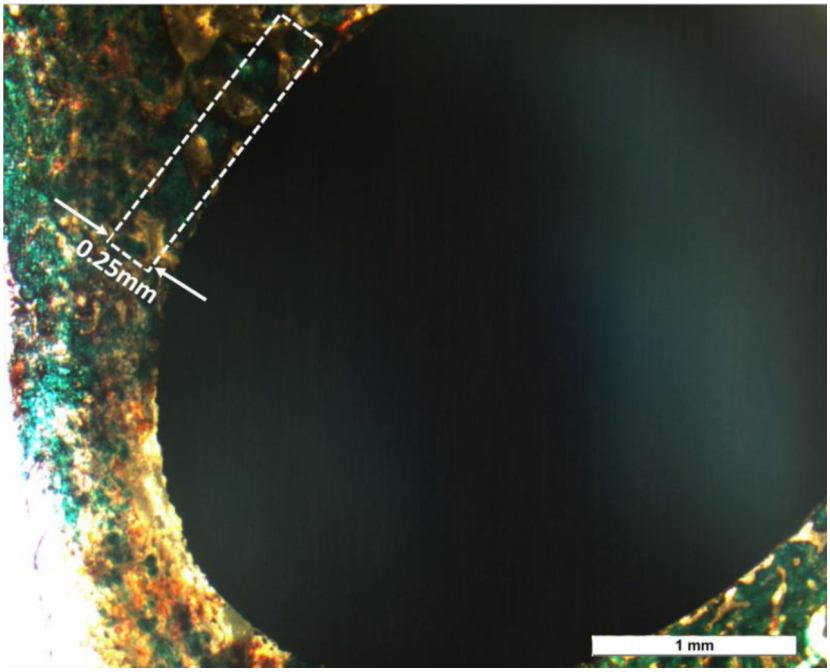

Fig. 2:

Histomorphometric analysis of the osteoid surface (OS) and mineralized bone surface (BS). Within a representative band around the implant (marked), that was 0.25mm thick, the red/orange area was calculated for OS/BS and the bluish-green area was calculated for MS/BS individually. The standard Histomorphometric evaluation was carried out following ASBMR standards.

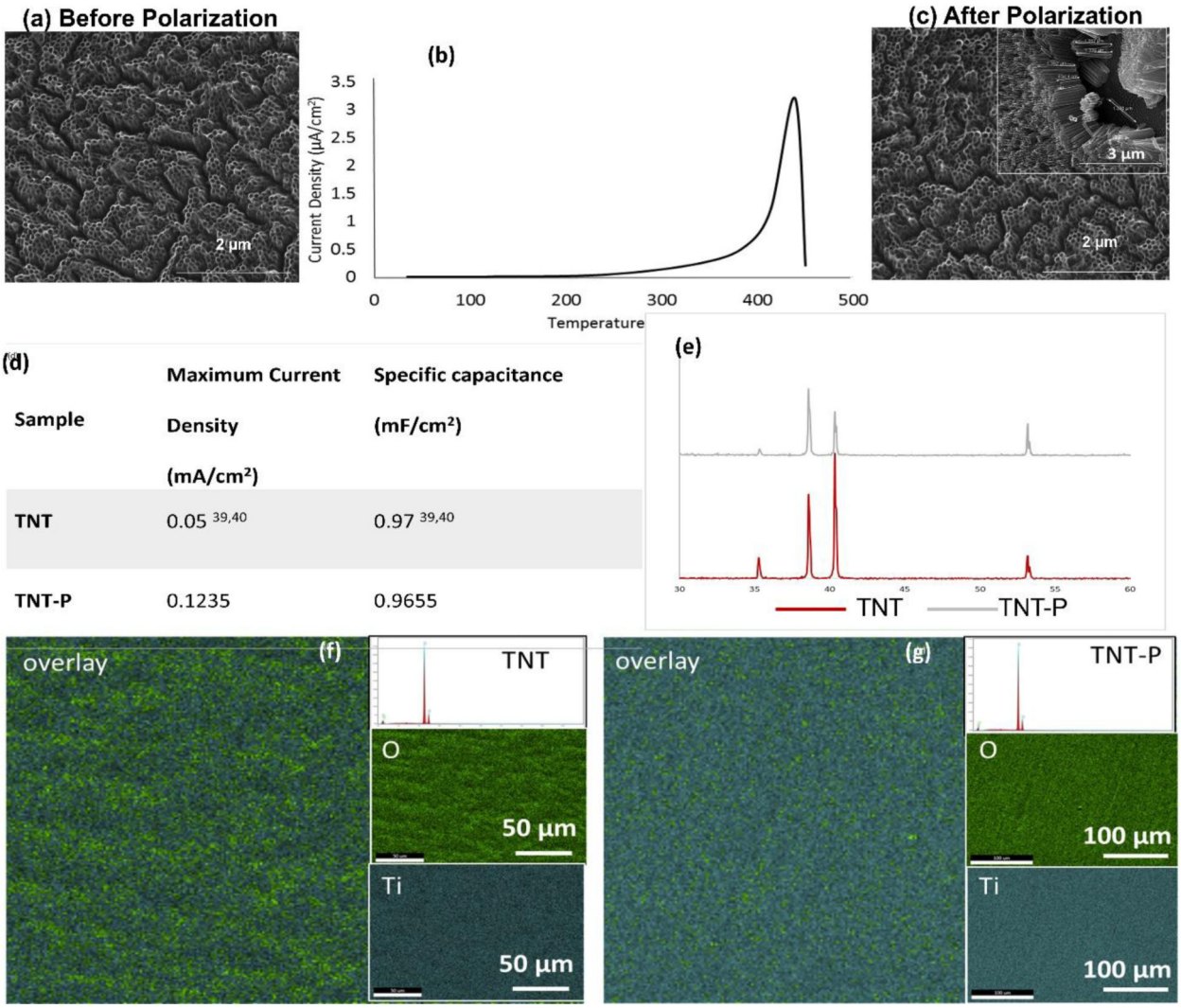

Fig. 3:

Material properties of the TNT-P. (a) and (c) show SEM micrograph of the nanoscale modification before and after the polarization was performed. No thermal degradation was noted in the nanotube array after the polarization. (b) TSDC spectrum of TNT polarized at 300°C. (d) shows comparison of specific capacitance and maximum current density values [39, 40] and (e) shows the XRD spectra of the TNT and TNT-P with no detection of secondary phases other than Ti due to the surface treatments. (g, f) represents surface chemical analysis using EDAX for TNT and TNT-P showing uniform distribution of Ti and O in the examined surface. Elemental composition spectrum shows no presence of contamination.

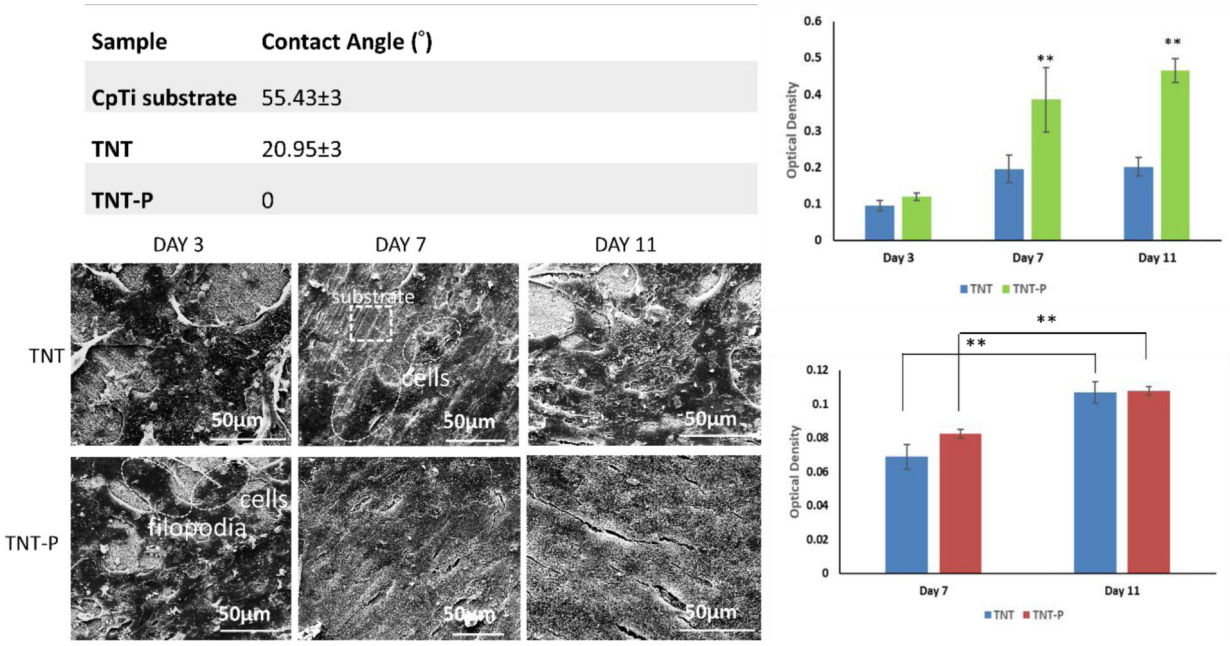

Fig. 4.

In vitro biological response of the surface treated Ti substrates. (a) Contact angle for all samples in D.I. water, demonstrating hydrophilic surface with TNT-P (b) MTT assay (c) ALP assay and (d) SEM micrographs, for TNT and TNT-P samples after 3, 7 and 11 days of culture. Statistical analyses were done using two-way ANOVA for n=9 and α=0.05. P-values <0.0001 were considered extremely significant (**). SEM micrographs show osteoblast attachment and proliferation on both compositions through the presence of filopodial extensions

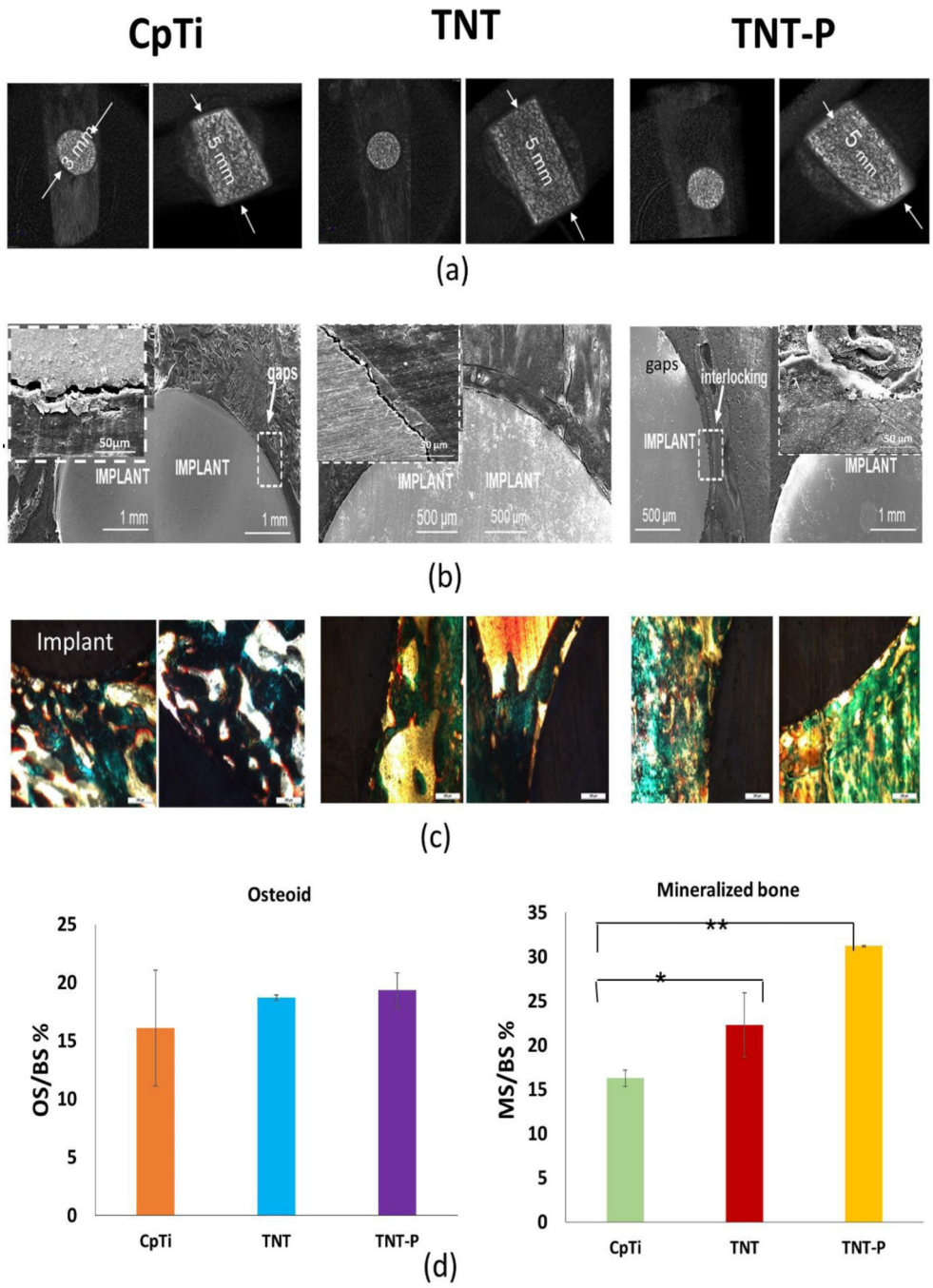

Fig. 5:

In vivo response of the surface treated Ti substrates in a rat distal femur model 5 weeks after implantation. (a) CT scan images exhibiting proper lodging of the implant into the femur bone of the animals (b) SEM micrographs of CpTi (inset – higher magnification image of an interfacial gap), TNT and TNT-P showing improved osseointegration through higher osseous tissue-implant interlocking for TNT-P and (c) optical micrographs for CpTi, TNT and TNT-P showing the presence of both osteoids like bone as well as mineralized bone formations d) Histomorphometric analysis of OS/BS and MS/BS around implants 5 weeks post-surgery.

The TNT-P samples show significantly higher mineralized bone in the vicinity of the implant as compared to the TNT and CpTi at an early 5-week time point. Osteoid surface was comparable between TNT and TNT-P and was higher than CpTi. ANOVA results for sample comparisons, n=6 and α=0.05. P-values between CpTi and TNT-P and between CpTi and TNT-P are less than 0.001 (significant*) and less than 0.0001 (extremely significant**), respectively.